# Design, Modeling and Control of T$^3$-Multirotor: a Tilting Thruster Type Multirotor*

Seung Jae Lee[1], Jaehyun Yoo[2] and H. Jin Kim[1]

***Abstract*— This paper presents a new design of multirotor, named as 'Tilting Thruster Type' (T$^3$)-multirotor. The new platform is equipped with mechanically separated thrusters, which can take any fuselage posture within a specified range regardless of any direction of translational acceleration. A specially designed servo-linkage mechanism is employed for relative attitude control between the thruster and the fuselage. Mathematical modeling and analysis of the new platform are conducted to explore the control method of the dynamically complex system. For demonstrating the potential of the new T$^3$-multirotor, an autonomous level flight is performed where the fuselage maintains zero roll and pitch angle during the entire flight. Both simulation and experimental results are provided with detailed analysis.**

## I. INTRODUCTION

The quadrotor, which behaves similarly to a helicopter but without complex operation principles, has become one of the representative aerial robot platforms due to its simple structure and uncomplicated dynamics. However, the oversimplification of the mechanism limits their capability in some cases. Of these, the biggest limitation is that the quadrotor can generate thrust only in the body z-direction due to the fixed motor mount. This makes the quadrotors an underactuated platform [1] that should tilt the entire fuselage to distribute body z-directional thrust to inertial X, Y, Z axes.

To address this underactuation problem, various concepts have been proposed. One line of research is to install thrust generators in multiple orientations [2]-[6]. The other line of research is to install some or all thrusters equipped with servo mechanisms to control the thrust direction during the flight [7]-[9]. Approaches of the first type have the advantage in terms of fully-actuated control in all attitude by combining multiple thrusters in various fixed directions. However, this type of multirotors suffers from efficiency since a significant portion of each motor thrust is spent to counteract the unwanted component vectors of the other motor thrusts. Also, some motors occasionally stop propeller rotation and become dead weight that does not participate in thrust generation. In the second type of approaches, specific thrust generators are tilted through the servo mechanism so that those thrusters produce the required acceleration in the desired direction, while most thrust generators are oriented vertically as in conventional multirotors. Therefore, it is more efficient compared with the first type while resolving the underactuation. However, the additional servo mechanisms for each and every thrust generator escalate both the mass and the power consumption rate of the platform.


Fig. 1. T$^3$-quadrotor whose upper part can tilt in roll and pitch direction. A servo mechanism (Lower Right) is designed to control the relative attitude between the upper and lower parts of the quadrotor.

In this paper, we present a new concept of quadrotor. Named as the Tilting Thruster Type multirotor (T$^3$-multirotor), it solves many problems of the conventional quadrotors that occur due to their underactuation by separating thrust generating part (TGP) and fuselage part (FP). As shown in figure 1, two parts are connected using a universal joint, which delivers X, Y, Z-directional force components and yaw-directional torsional force but liberates roll, pitch-directional torques. Therefore, any relative roll and pitch angle can be attained between TGP and FP. We install kinematic linkage at each of the two servo motors at the lower fuselage so that one side of linkage is attached to the horn of the servo motor while the other tip is connected to TGP. It allows us to control the relative roll and pitch angle between two parts by simple servo control. By solving the underactuation problem using only two servo motors, T$^3$-multirotor shows better efficiency compared to other competitive platforms.

This paper is structured as follows. Section II describes the detailed design and mechanism of the T$^3$-multirotor. In Section III, we present the mathematical model of the vehicle, and the detailed approach to control the platform in section IV. In Section V, we demonstrate the performance of

*This work was supported by the Robotics Core Technology Development Project (10080301) funded by the Ministry of Trade, Industry and Energy (MoTIE, Korea), National Research Foundation of Korea (NRF) grant funded by the Ministry of Science, ICT and Future Planning (2014M1A3A3A02034854).

[1]Seung Jae Lee and H. Jin Kim are with the Department of Mechanical and Aerospace Engineering and Automation and Systems Research Institute (ASRI), Seoul National University, Gwanak-gu, Seoul, Korea sjlazza@snu.ac.kr, hjinkim@snu.ac.kr

[2]Jaehyun Yoo is with the School of Electrical Engineering, KTH Royal Institute of Technology, Stockholm, Sweden jaehyun@kth.se


Fig. 2. The attitudinal behavior of the thrust generation part of actual T$^3$-quadrotor due to the servo angle ($\beta_2$) variation. Positive $\beta_2$ generates negative roll (Left), zero $\beta_2$ with zero roll (Middle), negative $\beta_2$ with positive roll attitude. During the $\beta_2$ movement, the pitch angle is not significantly changed.

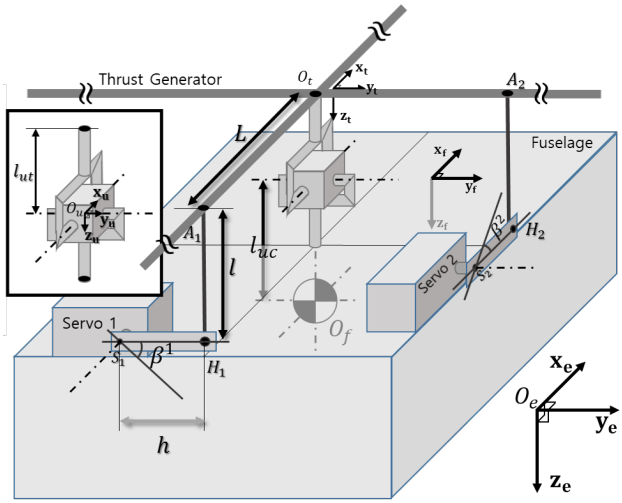


Fig. 3. A configuration diagram of T$^3$-multirotor. Universal joint mechanism enables attitudinal freedom in $\phi_t^f$ and $\theta_t^f$ while two servo systems with tie rod linkage control free the attitude components with physical constraints.

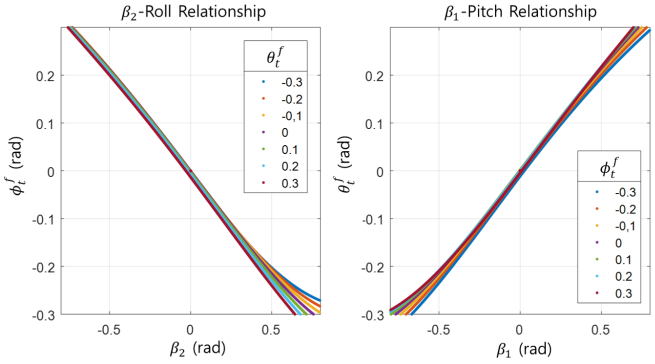


Fig. 4. Map between $\beta_2$ (Servo 2 angle) and $\phi_t^f$ (Left), $\beta_1$ (Servo 1 angle) and $\theta_t^f$ (Right) in various residual attitude factor condition.

the T$^3$-multirotor by using both simulation and experimental results.

## II. MECHANICAL DESIGN

In this section, we detail the design of T$^3$-multirotor. We first define the symbols described in Fig. 3. The $\mathcal{F}_e = \{x_e, y_e, z_e\}$ with origin at $O_e$ describes the earth-fixed frame, while $\mathcal{F}_f = \{x_f, y_f, z_f\}$ with origin at $O_f$ is the body-fixed frame attached to the fuselage where $O_f$ is located on the center of mass (COM) of the fuselage part (FP). The frame $\mathcal{F}_u = \{x_u, y_u, z_u\}$ has its origin $O_u$ at the center of the universal joint. $\mathcal{F}_t = \{x_t, y_t, z_t\}$ with origin at $O_t$ is the TGP-attached body-fixed frame. $\mathcal{F}_f$ and $\mathcal{F}_u$ are identical except for the location of the origin. The positions of FP and TGP with respect to the earth-fixed frame are denoted by $p_f, p_t \in \mathbb{R}^3$ and the attitudes $\Theta_t, \Theta_f \in SO(3)$, where $p_* = [x_*\ y_*\ z_*]^T$ and $\Theta_* = [\phi_*\ \theta_*\ \psi_*]^T$. $S_1$ and $S_2$ are the positions of the rotation center of each servo motor. $H_1, H_2$ and $A_1, A_2$ are the rod-end positions of the tie rods, where $H_*$ denotes the attach point of the servo horn and $A_*$ the attach point on the TGP. The length of the tie rod is $l$, while $\overline{O_tA_*}$ is $L$, $\overline{O_fO_u}$ is $l_{uc}$ and $\overline{O_uO_t}$ is $l_{ut}$. $h$ is the length of the servo horn. The angles of servo 1 and servo 2 are $\beta_1 \in \mathbb{R}$ and $\beta_2 \in \mathbb{R}$ respectively.

Let $(\bullet)^*$ denote the quantity $\bullet$ with the point of view from the starred frame. With help of the universal joint mechanism located between TGP and FP, we can freely choose $\Theta_t^f = [\phi_t^f\ \theta_t^f\ \psi_t^f]^T$, the relative attitude between TGP and FP, except for the relative yaw. As depicted in Fig. 3, $\Theta_t^f$ is controlled by two servo motors connected by a kinematic link. More specifically, the position of $A_*$ changes with the variation of servo angle $\beta_*$ because the distance between $A_*$ and $H_*$ is fixed by the tie-rod. The T$^3$-multirotor's kinematic link is designed for each servo motor to control the $\phi_t^f$ and $\theta_t^f$ independently. In particular, $\beta_1$ is designed to dominantly control $\theta_t^f$, while $\beta_2$ is designed to dominantly control $\phi_t^f$. Fig. 4 is an experimental result showing the relationship between $\beta$ and $\Theta_t^f$. As shown in the left graph, the relationship between $\beta_2$ and $\phi_t^f$ is almost

linear within a certain range with respect to various values of $\beta_1$. A similar phenomenon is also observed in the $\beta_2$-$\theta_t^f$ relationship.

## III. MODELLING

In this section, we build a mathematical model of T$^3$-multirotor. To fully analyze and simulate the behavior of the T$^3$-multirotor with relatively complex dynamic characteristics, a different approach is required instead of a simplified dynamic model for conventional multirotors. However, in case of exploring the actual control method of the platform, a simplified dynamic analysis may be better because many state variables can simply be measured through the attached sensors. In this section, we present two types of dynamic analysis, where the first investigation covers full model dedicated for simulation and the second investigation covers relatively simple analysis but better suited to provide an intuition on how to control our platform.

### A. Dynamics:Udwadia-Kalaba Approach

Recently, a modeling method called Udwadia-Kalaba (U-K) approach [10] is becoming popular to solve dynamically coupled systems, which we employ in this section. Consider the dynamics of an unconstrained system

$$M\ddot{q}_u = Q \tag{1}$$

where $M \in \mathbb{R}^{n\times n}$ is a (symmetric) positive definite generalized mass matrix, $\ddot{q}_u \in \mathbb{R}^n$ is the acceleration vector describing the unconstrained movement of the object, $Q \in \mathbb{R}^n$ is a generalized force vector. When the system is subject to $m$ constraints that are represented by sufficiently smooth equations, we can differentiate them to obtain the following form :

$$A(q,\dot{q},t)\ddot{q} = b(q,\dot{q},t) \tag{2}$$

where $\ddot{q} \in \mathbb{R}^n$ is the acceleration vector describing the constrained movement of the object. $A = [A_1\ A_2\ \cdots\ A_m]^T \in \mathbb{R}^{m\times n}$, $b = [b_1\ b_2\ \cdots\ b_m]^T \in \mathbb{R}^m$ are the matrices obtained by differentiation of the $m$ constraints.

Considering the physical constraint, equation (1) becomes

$$M\ddot{q} = Q + Q_c \tag{3}$$

where $Q_c \in \mathbb{R}^n$ is the constraint force that hinders the unconstrained behavior $\ddot{q}_u$. Based on the U-K equation [10], $Q_c$ is calculated with

$$Q_c = M^{1/2}(AM^{-1/2})^{+}(b - A\ddot{q}_u). \tag{4}$$

The $(\cdot)^+$ symbol describes the Moore-Penrose pseudoinverse. Then, the constrained movement of the object is described as

$$\ddot{q} = \ddot{q}_u + M^{-1/2}(AM^{-1/2})^{+}(b - A\ddot{q}_u). \tag{5}$$

In our case, there are two constraints to consider: the yaw angle constraint and the relative distance constraint.

*1) Yaw angle constraint:* The first constraint represents that the yaw angles of TGP and FP must always be the same due to the rotational constraint of the universal joint. First, we define the yaw angle difference between TGP and FP as

$$\Delta_y = Z^e(\Theta_t^e - \Theta_f^e) \tag{6}$$

where $Z^e = [0\ 0\ 1]$. Then, we build a constraint equation $\Gamma_y$ as

$$\Gamma_y = \Delta_y - E_y \tag{7}$$

where $E_y$ represents the desired yaw angle error between the two parts, which is zero in our case. Differentiating $\Gamma_y$ twice and by organizing the resulting $\ddot{\Gamma}_y$, we get the constraint matrices $A_y$ and $b_y$.

*2) Relative distance constraint:* The second constraint is due to the condition that TGP and FP must always be in contact with the universal joint. First, we define the distance between two attach points as

$$\Delta_p = (p_t^e + R(\Theta_t^e)p_u^t) - (p_f^e + R(\Theta_f^e)p_u^f). \tag{8}$$

Then, we build a constraint equation $\Gamma_p$ as

$$\Gamma_p = ||\Delta_p||^2 = \Delta_p^T\Delta_p - E_p^2. \tag{9}$$

where $E_p$ represents the desired distance between the two parts, which is also zero in our case. Same as the case for $\Gamma_y$, we differentiate $\Gamma_p$ twice to get the constraint matrices $A_p$ and $b_p$.

Through the above two constraints, we obtain the matrices $A$ and $b$ needed for the construction of equation (2) as

$$A = \begin{bmatrix} A_y \\ A_p \end{bmatrix} \qquad b = \begin{bmatrix} b_y \\ b_p \end{bmatrix}. \tag{10}$$

These matrices are used to calculate the constraint force $Q_c$ in equation (4). Since the two constraints are related to relative posture and position respectively, we choose $q = [p_t\ \Theta_t\ p_f\ \Theta_f]^T_{1\times 12}$ to fully reflect the system. Now, we combine the mechanism derived from the universal joint with the servo mechanism to derive the full model of the T$^3$-quadrotor. Recall that the purpose of the servo mechanism is to give pushing and pulling force to the $A^f$ point in order to generate proper torque for $\Theta_t^f$ control. Therefore, it is possible to cause an equivalent behavior by giving sufficient torque directly to $\mathbf{x}_u$ and $\mathbf{y}_u$ axes in Fig. 3. If we define those two equivalent torques as $\tau_x$ and $\tau_y$, they act on both TGP and FP in the opposite direction due to the Newton's third law of motion. It can be written as the following generalized force vector form

$$Q_t = [0_{1\times 3}\ [-\tau_{s,y}\ -\tau_{s,x}\ 0]\ 0_{1\times 3}\ [\tau_{s,y}\ \tau_{s,x}\ 0]]^T_{1\times 12}. \tag{11}$$

The full model is then

$$M_T\ddot{q} = Q_T + Q_c + Q_t \tag{12}$$

where $M_T$ is a generalized mass matrix. The value of $Q_T$ in the equation of motion correponds to the case when there is no constraint between TGP and FP. For TGP, the general multirotor dynamic equation is employed, while only

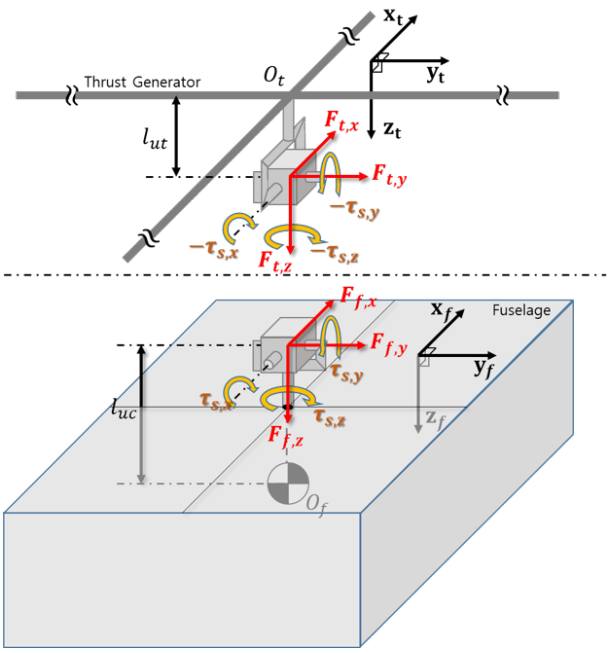


Fig. 5. Isolated configuration diagram. Internal force and servo torque are indicated.

gravitational acceleration is considered for FP which cannot generate thrust by itself.

Through this dynamic analysis, we are able to obtain the dynamic equation (12) that takes both the coupling factor and servo torque between TGP and FP into account. The next subsection covers the second dynamic analysis to find out how to achieve the desired control.

### B. Dynamics:Free Body Diagram Analysis

In this subsection, we discuss dynamic analysis based on a free body diagram (FBD). Through the analysis, we aim to find the methodology to control the attitude of the dynamically coupled TGP and FP independently.

For the FBD-based model analysis, first, we isolate the thrust generator part and the fuselage part. In the process of isolating the two parts, the dynamic coupling between them is considered by marking each FBD with the internal force generated by the universal joint and the torque generated by the servo mechanism. Then, we establish the dynamic equation for each part from the FBD. To simplify the modeling process, we introduce the virtual relative attitude control torque $\tau_s = [\tau_{s,x}\ \tau_{s,y}\ \tau_{s,z}]^T$ which produces an equivalent effect to the torque generated by the servo motor mechanism. Note that unlike $\tau_x$ or $\tau_y$, we cannot control $\tau_z$. Instead, $\tau_z$ is determined by universal joint's axial rotation constant. Fig. 5 shows the top and bottom parts of each FBD with servo-generated $\tau$ and the internal force $F$.

*1) Dynamics-TGP:* TGP itself is capable of generating thrust $T_t = [0\ 0\ -\Sigma F_i]^T$ and torque $\tau_t = [\tau_{t,x}\ \tau_{t,y}\ \tau_{t,z}]^T$, where those two quantities are defined with respect to the $\mathcal{F}_t$ coordinate system. $F_i,\ i = 1, 2, \cdots, n$ are the propulsive forces generated by each of $n$ propellers of the T$^3$-multirotor. The dynamic equations of the TGP is then

$$R(\Theta_t^e)\,(T_t + F_t) + M_t\vec{g} = M_t\ddot{p}_t \tag{13}$$

$$\begin{aligned}\tau_{t,total} &= \tau_t + (-\tau_s) + \vec{\lambda}_{ut} \times F_t \\ &= J_t\dot{\Omega}_t + \Omega_t \times (J_t\Omega_t)\end{aligned} \tag{14}$$

where $M_t$ is the mass of TGP, $\vec{g} = [0\ 0\ g]^T$ is the gravitational acceleration vector and $p_t$ is the position vector of the TGP measured from $\mathcal{F}_e$ as defined before. $\tau_{t,total}$ is the total external torque applied to TGP, $\vec{\lambda}_{ut} = [0\ 0\ l_{ut}]^T$ is the vector from $O_t$ to $O_u$. $J_t$ is the moment of inertia (MOI) of TGP, and $\Omega_t$ is the body angular velocity of TGP.

*2) Dynamics-FP:* Compared with TGP, FP does not have its own propulsion system. Except for gravity, the only external inputs of FP are $F_f$ and $\tau_s$. Therefore, the dynamic equations that reflect the external inputs are

$$R(\Theta_f^e)F_f + M_f\vec{g} = M_f\ddot{p}_f \tag{15}$$

$$\begin{aligned}\tau_{f,total} &= \tau_s + \vec{\lambda}_{uc} \times F_f \\ &= J_f\dot{\Omega}_f + \Omega_f \times (J_f\Omega_f)\end{aligned} \tag{16}$$

where $M_f$ is the mass of the FP and $p_f$ is the position vector of the FP. $\tau_{f,total}$ is the total external torques applied to FP, $\vec{\lambda}_{uf} = [0\ 0\ -l_{uf}]^T$ is the vector from $O_f$ to $O_u$. $J_f$ is the MOI of FP, $\Omega_f$ is the body angular velocity of FP.

Through the second dynamic analysis, it is obvious that $\tau_{t,total}$ and $\tau_{f,total}$ should be controlled appropriately for independent attitude control of TGP and FP. However, the actual controllable elements are the $\tau_t$ and $\tau_s$ where $\tau_t$ is generated from the TGP's motors and $\tau_s$ by the servo motor. Therefore, in the next section, we will deal with a control technique that properly controls $\tau_t$ and $\tau_s$ to make $\tau_{t,total}$ and $\tau_{s,total}$ equal to our desired values.

## IV. CONTROL

Prior to discussion on control, we note that $F_t$ and $F_f$ are terms in an action-reaction relationship expressed by the following equation :

$$R(\Theta_t^e)F_t + R(\Theta_f^e)F_f = 0. \tag{17}$$

The estimated $F_f$ is obtained from the equation (15) as

$$\hat{F}_f = M_f R^{-1}(\Theta_f^e)\,(\ddot{p}_f - \vec{g}) \tag{18}$$

where $\Theta_f^e$ and $\ddot{p}_f$ are measurable through an IMU mounted on the FP. Combining equations (17) and (18), we get

$$\hat{F}_t = -R^{-1}(\Theta_t^e)R(\Theta_f^e)F_f \tag{19}$$

where the direct calculation of $F_t$ through equation (13) is not possible because $T_t$ cannot be measured. On the unavailability of $T_t$, refer [11]. The quantity $\Theta_t^e$ is measured through the IMU on the TGP as in the case of FP.

Now, we discuss methods for controlling $\Theta_t^e$ and $\Theta_f^e$. As discussed earlier, proper values of $\tau_{t,total}$ and $\tau_{f,total}$ should be generated to control the attitude of TGP and TP individually. However, only $\tau_t$ and $\tau_s$ are the inputs that we can control. Therefore, we need to find a way to control $\tau_t$ and $\tau_s$ that produce $\tau_{t,total}$ and $\tau_{f,total}$ as desired. Fig. 6

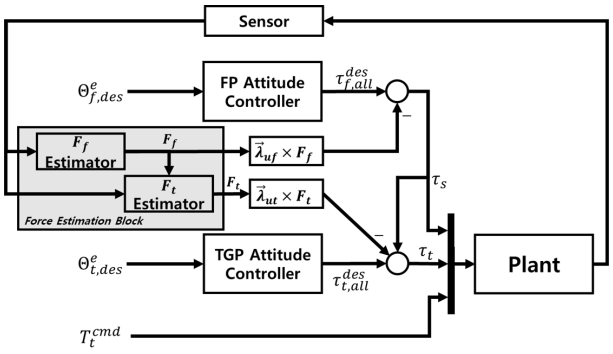


Fig. 6. Signal flow diagram of a control scheme for performing independent attitude control of TGP and FP.

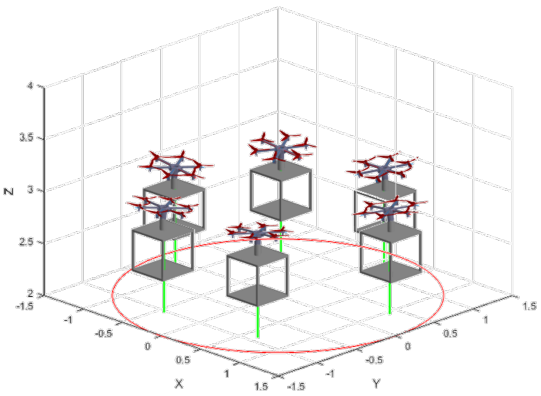


Fig. 7. Flight simulation of the T$^3$-multirotor. The thrust generation part tilts during the flight while fuselage part remains level.

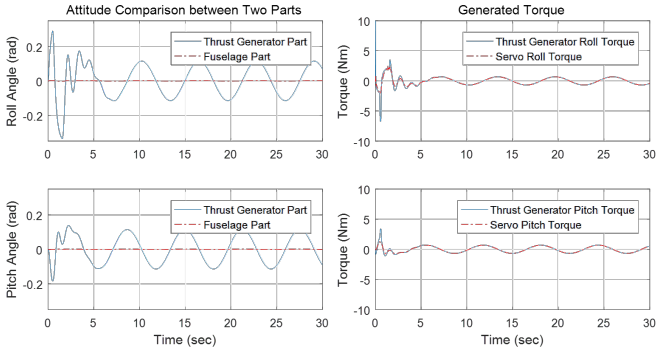


Fig. 8. Simulation results on zero roll and pitch control of fuselage part. Roll and pitch angles of TGP and FP (Left), and roll and pitch torques generated by propellers and servo mechanism (Right).

shows the overall control structure of T$^3$-multirotor. Similar to a conventional multirotor control, $\Theta^e_{t,des}$, $\Theta^e_{f,des}$ and $T_t$ command are generated from an outer-loop controller. Once the control inputs are generated, separate attitude controllers that are responsible for FP and TGP respectively compute the desired signals $\tau^{des}_{f,total}$ and $\tau^{des}_{t,total}$. Meanwhile, the 'Force Estimation Block' in Fig. 6 continuously estimates $F_t$ and $F_f$ based on the equation (18) and (19). Once the internal forces are estimated, we are now ready to calculate the appropriate values for $\tau_t$ and $\tau_s$ in order to make $\tau_{t,total}$ and $\tau_{f,total}$ equal to their desired values $\tau^{des}_{t,total}$ and $\tau^{des}_{f,total}$. From equation (14) and (16), we can write $\tau_s$ and $\tau_t$ as

$$\tau_s = \tau^{des}_{f,total} - \vec{\lambda}_{uc} \times \hat{F}_f \tag{20}$$

$$\tau_t = \tau^{des}_{t,total} + \tau_s - \vec{\lambda}_{ut} \times \hat{F}_t. \tag{21}$$

First, we calculate $\tau_s$ by compensating the moment due to the internal force (i.e. the second term on the right hand side of equation (20)) from $\tau^{des}_{f,total}$. Once we obtain $\tau_s$, we calculate $\tau_t$ by compensating the effects of $\tau_s$ and the moment due to the internal force (i.e. the third term on the right hand side of equation (21)). Combining equations (20) and (21) with (14) and (16), we can see that

$$\tau_{f,total} = \tau^{des}_{f,total} + \vec{\lambda}_{uf} \times (F_f - \hat{F}_f) \approx \tau^{des}_{f,total} \tag{22}$$

$$\tau_{t,total} = \tau^{des}_{t,total} + (\tau_s - \tau_s) + \vec{\lambda}_{ut} \times (F_t - \hat{F}_t) \approx \tau^{des}_{t,total} \tag{23}$$

## V. SIMULATION AND EXPERIMENT

This section presents the simulation and experimental result of T$^3$-multirotor flight. As mentioned earlier in section III, the dynamic equations derived from the UK equations are used for the simulation.

### A. Simulation

The simulation of T$^3$-multirotor is performed on full dynamics equations (12) to check whether we can operate the system as desired. During the simulation, the T$^3$-multirotor flies on a circular path shown in Fig. 7 which constantly requires to change the attitude for trajectory tracking. While the thrust generation part changes its attitude by controlling the rotation speed of motors, $Q_t$ in equation (11) is properly controlled to keep the attitude of the fuselage part steady. The left figures of Fig. 8 show roll and pitch attitude of two parts of T$^3$-multirotor with respect to the earth-fixed frame for 30 seconds of simulation. The right figures show the generated torque of each part of T$^3$-multirotor. At the initial state, it makes huge control input to follow the circular path as fast as possible. Therefore the torque produced by the thrust generation part shows large value in both roll and pitch axes. Meanwhile, the servo roll and pitch torques are generated by the relative angle controller that tries to make the fuselage part level during the flight. It is noticeable that after around 5 seconds, the torque generated by the thrust generation part and servo torque become equalized. It confirms that the overall mechanism is working correctly by cancelling the effect on FP coming from TGP using the servo motor, thus allowing the FP to maintain zero roll and pitch.

### B. Experiment

The experiment of T$^3$-multirotor is performed with the custom-made quadrotor type aerial vehicle. Fig. 9 shows the comparison between the flight without $\Theta^f_t$ control and with $\Theta^f_t$ control. As we see in the upper picture, it behaves same as the conventional underactuated multirotors that need to change the attitude for generating the desired acceleration

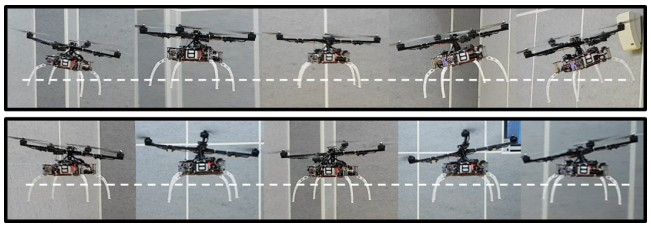

Fig. 9. The comparison between two cases of flight scenarios. The first instance (shown in the upper snapshots) demonstrates the flight with the fixed relative attitude, i.e. the relative roll and pitch are zero, same as common multirotors. The second instance (lower snapshots) demonstrates the flight with controlled relative attitude, where the attitude of the fuselage part remain level regardless of the horizontal movement of the platform.

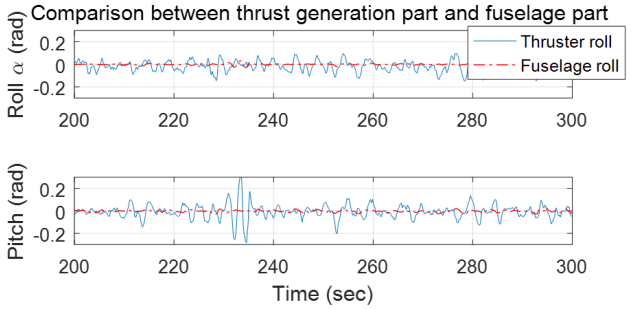


Fig. 10. The attitude comparison between the thrust generation part and the fuselage part.

vector. However, as in the lower picture, the fuselage part of the T$^3$-quadrotor remains level regardless of the translational movement, as the relative attitude $\Theta_t^f$ is properly controlled by the servo angle control. Fig. 10 is an attitude comparison between the thrust generation part and fuselage part. As we see, the attitude of the fuselage remains near zero during the flight while the thrust generation part consistently changes the attitude to generate the desired translational acceleration.

To demonstrate the benefits of T$^3$-multirotor design, another experiment was conducted. For many rotary aircraft, taking off from the sloped ground is highly dangerous. The reason is that most of the rotorcraft's thrust direction is fixed to the vertical direction of the fuselage, so the thrust is generated in its vertical direction to the slope. Inclined thrust generation accelerates the fuselage in the horizontal direction, creating a large horizontal motion that could cause the aircraft to roll over or even crash in extreme cases. However, in the case of T$^3$-multirotor, the direction of thrust can be determined independently of the fuselage where the landing gear is attached, making it possible to take off stably even on a sloped area. See Fig. 11 for experimental results.

## VI. CONCLUSIONS

This paper introduced a new design of a fully-actuated multirotor called T$^3$-multirotor, where the fuselage has a full degree of freedom in any flyable condition. To build a non-underactuated multirotor, we designed a platform consisting of two major parts of thrust generation and fuselage, where the universal joint located between them provides freedom

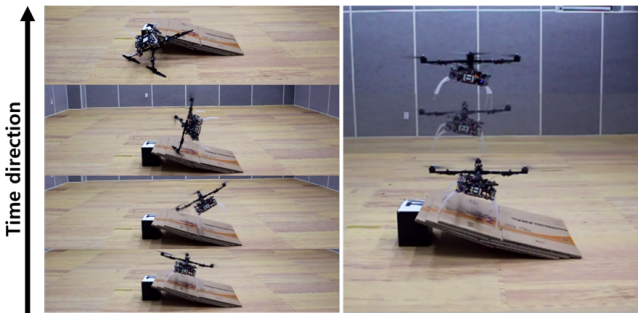


Fig. 11. Comparison of slope takeoff between conventional multirotor (Left) and T$^3$-multirotor (Right).

in the relative roll and pitch attitude while those angles are controlled by the servo-linkage. We performed mathematical modelling of the proposed multirotor design using U-K equation for full consideration of physical constraints. Both simulation and experiment are conducted to verify the feasibility of the concept. By using the ability to control the relative position between thrust generation part and fuselage part, we expect that T$^3$-multirotor can be applied in various scenarios such as take-off and landing on a slope, transportation of additional heavy payload, installing various payload sensors without extra systems like gimbals, which are difficult or impossible for conventional under-actuated multirotors.

## REFERENCES


[1] Huang, Mu, et al. "Adaptive tracking control of underactuated quadrotor unmanned aerial vehicles via backstepping." American Control Conference (ACC), 2010. IEEE, 2010.

[2] Brescianini, Dario, and Raffaello D'Andrea. "Design, modeling and control of an omni-directional aerial vehicle." Robotics and Automation (ICRA), 2016 IEEE International Conference on. IEEE, 2016.

[3] Jiang, Guangying, and Richard Voyles. "A nonparallel hexrotor UAV with faster response to disturbances for precision position keeping." Safety, Security, and Rescue Robotics (SSRR), 2014 IEEE International Symposium on. IEEE, 2014.

[4] Langkamp, D., et al. "An engineering development of a novel hexrotor vehicle for 3D applications." International Micro Air Vehicle conference and competitions 2011 (IMAV 2011),'t Harde, The Netherlands, September 12-15, 2011. Delft University of Technology and Thales, 2011.

[5] Salazar, Sergio, et al. "Modeling and real-time stabilization of an aircraft having eight rotors." Unmanned Aircraft Systems. Springer Netherlands, 2008. 455-470.

[6] Park, Sangyul, et al. "Design, modeling and control of omni-directional aerial robot." Intelligent Robots and Systems (IROS), 2016 IEEE/RSJ International Conference on. IEEE, 2016.

[7] Ryll, Markus, Davide Bicego, and Antonio Franchi. "Modeling and control of FAST-Hex: a fully-actuated by synchronized-tilting hexarotor." Intelligent Robots and Systems (IROS), 2016 IEEE/RSJ International Conference on. IEEE, 2016.

[8] Ryll, Markus, Heinrich H. Blthoff, and Paolo Robuffo Giordano. "A novel overactuated quadrotor unmanned aerial vehicle: Modeling, control, and experimental validation." IEEE Transactions on Control Systems Technology 23.2 (2015): 540-556.

[9] Kastelan, D., M. Konz, and J. Rudolph. "Fully Actuated Tricopter with Pilot-Supporting Control" IFAC-PapersOnLine 48.9 (2015): 79-84.

[10] Udwadia, Firdaus E., and Robert E. Kalaba. A new perspective on constrained motion. Proceedings: Mathematical and Physical Sciences (1992): 407-410.

[11] Lee, Seung Jae, et al. "Robust acceleration control of a hexarotor UAV with a disturbance observer." Decision and Control (CDC), 2016 IEEE 55th Conference on. IEEE, 2016.